Estuarine, Coastal and Shelf Science 262 (2021) 107574

Contents lists available at ScienceDirect

Estuarine, Coastal and Shelf Science

journal homepage: www.elsevier.com/locate/ecss

Quantifying natural sediment erodibility using a mobile oscillatory flow channel☆

J.C. de Smit [a,b,*], M.G. Kleinhans [b], T. Gerkema [a], T.J. Bouma [a,b]

[a] NIOZ Royal Netherlands Institute for Sea Research, Department of Estuarine and Delta Systems, Yerseke, the Netherlands
[b] Faculty of Geosciences, Department of Physical Geography, Utrecht University, Utrecht, the Netherlands

ARTICLE INFO

Keywords:
Cohesive sediment
Erodibility
Estuary
Shear stress
Tidal flat
Waves

ABSTRACT

Erosion of tidal flats is to a large degree determined by the erosion threshold of their cohesive sediments, i.e., the critical bottom shear stress identifying the onset of erosion. Given that the erodibility of tidal flats can vary strongly over both space and time, rapid in situ measuring methods for quantifying the critical bottom shear stress are needed. As the largest changes in tidal flat elevation are generally observed during storms when shear stress is wave dominated, we developed a mobile Oscillatory-Channel Resuspension flume, OsCaR, as a rapid method to measure the critical wave-generated shear stress on sediment cores directly taken from the field. We assessed the performance of the OsCaR-flume by conducting erodibility measurements on a range of artificial sand – mud mixtures, and along a natural longshore estuarine sediment type and benthic assemblage gradient. Measured erodibility of the artificial sediments matched well with sediment transport theory, indicating that the OsCaR-flume is able to reproduce wave-generated shear stress accurately. Moreover, the patterns observed in the influence of total benthic metabolic rate divided over functional groups on sediment erodibility show that the OsCaR-flume is able to capture the main benthic processes, as they corresponded well to previous laboratory based studies.

1. Introduction

Tidal flats are living landscapes, of which the morphodynamics are governed by the interaction between benthos and the deposition and erosion of sediments. Sediment dynamics of tidal flats are an important process for the morphological and ecological development of estuaries as a whole. For example, eroding tidal flats can cause cliff formation at the salt marsh boundary (Bouma et al., 2016), and increase the exposure of these cliffs to waves (Mariotti and Fagherazzi, 2010). On the other hand, stable tidal flat sediments may provide windows of opportunity for settlement of pioneer salt marsh species (Hu et al., 2015). Besides these short-term impacts, tidal flat erodibility also drives the large-scale, long-term morphological development of estuaries (Braat et al., 2017; Brückner et al., 2021).

Tidal flat sediments generally consist of a mixture of sand (grain size between 63 μm and 2 mm), silt (grain size between 4 μm and 63 μm), and clay (grain size below 4 μm). Silt and clay are typically considered as a single mud fraction. When the mud fraction is sufficient, the sediment becomes cohesive (Mitchener and Torfs, 1996; van Ledden, 2003). The erosion rate (E, kg m^{-2} s^{-1}) of consolidated cohesive sediments can be described as a function of a critical bottom shear stress for the onset of erosion (τ_{cr}, N m^{-2}; also referred to as critical erosion threshold), the actual occurring bottom shear stress (τ, N m^{-2}), and an erosion parameter (E_0, kg m^{-2} s^{-1}) which describes the erosion rate once τ_{cr} is exceeded (Partheniades, 1965):

$$E = E_0\left(\frac{\tau}{\tau_{cr}} - 1\right),\ if\ \tau > \tau_{cr},\ else\ E = 0 \quad [1]$$

While eq. (1) does not account for important processes such as the increase of bed strength with erosion depth, variations of this equation are widely used in (bio)geomorphological modelling under the assumption that the missing effects are compensated for in the coefficients (Mehta et al., 1989; Braat et al., 2017; Brückner et al., 2021). The high sensitivity of the erosion rate (E) to critical bottom shear stress (τ_{cr}) makes it crucial to accurate quantify τ_{cr} of natural sediments in order to predict the morphodynamic development of tidal flats.

☆ The authors have contributed to this manuscript as following in terms of study design / conducting measurements / flume development / data analysis / manuscript writing: JCdS (50/100/40/60/70), MGK (20/0/20/15/10), TG (10/0/20/10/10), TJB (20/0/20/15/10).

* Corresponding author. NIOZ Royal Netherlands Institute for Sea Research, Department of Estuarine and Delta Systems, Yerseke, the Netherlands.
E-mail address: jaco.de.smit@nioz.nl (J.C. de Smit).

https://doi.org/10.1016/j.ecss.2021.107574
Received 17 May 2021; Received in revised form 23 July 2021; Accepted 3 September 2021
Available online 10 September 2021
0272-7714/© 2021 The Author(s). Published by Elsevier Ltd. This is an open access article under the CC BY license (http://creativecommons.org/licenses/by/4.0/).

The critical bottom shear stress of tidal flat sediments is strongly influenced by the presence of benthos, provided that the sediment is cohesive (Li et al., 2017). In general, microphytobenthos stabilize the sediment by excreting extracellular polymeric substances EPS, whereas bioturbating macrozoobenthos generally destabilize the sediment through modification of the sediment structure (Paterson and Black, 1999). The density and species composition of benthos is highly variable over both space and time, due to e.g. variations in sediment grain size (Ysebaert and Herman, 2002; Cozzoli et al., 2013). As a result, tidal flat erodibility is also highly site specific (Joensuu et al., 2018) and is subjected to large spatial and temporal differences, which are difficult to predict (Widdows et al., 2000; Zhu et al., 2019). Hence there is need to be able to measure the critical bottom shear stress of tidal flat sediments in an easy and fast way under realistic conditions.

Two types of methods have been developed so far to measure τ_{cr} of natural sediments: *i)* devices that generate a shear force on the bed by simulating turbulent flow through vertical jets or propellers (Schünemann and Kühl, 1993; Tolhurst et al., 1999), and *ii)* devices capable of generating natural flow conditions, such as in situ annular flumes (Amos et al., 1992; Widdows et al., 1998), or unidirectional flow channels (Houwing and Van Rijn, 1998). Devices that simulate turbulent flow are generally small, and therefore easy to deploy. This makes them suitable for conducting high numbers of replicated measurements (Tolhurst et al., 1999), but unrealistic in terms of shear stress generation (Widdows et al., 2007). The advantage of annular flumes is that they are able to generate a horizontal shear stress, i.e., similar to natural flow conditions, which provides more reliable τ_{cr} measurements. Albeit that the annular shape yields secondary flows which cause significant variation in bed shear stress across the sediment surface, and makes it impossible to correctly orientate bed forms with respect to the flow direction throughout the channel. Another drawback is that they can be difficult to deploy. Annular flumes often require transplantation of the sediment into the flume, and in situ unidirectional flow channels need to be fully submerged. As a result, they are generally used for process studies rather than large scale monitoring of τ_{cr}.

A limitation to the existing methods to measure τ_{cr} using a horizontal shear stress, is that they are based on unidirectional flow. Tidal flow, which be assumed unidirectional on the timescale of an erodibility measurement, is indeed the dominant hydrodynamic forcing on tidal flats under average conditions. But it typically promotes sediment accretion, if there is sufficient sediment availability, as the hydrodynamic energy on the tidal flat is lower than in the tidal channel (Yang et al., 2003). Erosion due to tidal flow on muddy tidal flats is generally limited to millimeters (Hu et al., 2015; de Vet et al., 2020). Instead, the largest erosional events are generally observed during storms, when hydrodynamic energy on the tidal flats exceeds that of the tidal channel, specifically at water depths where waves become depth limited and thereby locally generate high shear stresses (Yang et al., 2003; Hu et al., 2015; de Vet et al., 2020).

Recently an in situ oscillatory flow channel, the TiDyWAVE, has been introduced (de Smit et al., 2020) to be able to measure τ_{cr} for both bare and vegetated sediments. The use of TiDyWAVE has similar limitations as annular and unidirectional flow channels in terms of ease of deployment, limiting its applicability for large-scale spatial-explicit quantification of τ_{cr} on tidal flats. We therefore introduce a flume design specifically catered to assessing tidal flat erodibility of natural sediments without aboveground benthic structures, from small and easy to take sediment cores: the Oscillatory-Channel Resuspension flume (OsCaR--flume). In this study we assess the hydrodynamic performance of the OsCaR-flume by *i)* conducting erodibility measurements of a range of defaunated sand-mud mixtures, in order to assess the hydrodynamic performance of the OsCaR-flume against proven flume setups that are used to study sediment erodibility, and *ii)* conducting erodibility measurements along a natural longshore estuarine gradient, in order to assess the performance of the OsCaR-flume when measuring natural sediments containing a variety of benthic invertebrates and bed forms.

2. Materials and methods

2.1. Flume description and design considerations

The OsCaR-flume is based on oscillatory flow tunnels (also known as U-tubes), which are used for studying sediment dynamics and near-bed hydrodynamics under full-scale ocean waves (O'Donoghue and Clubb, 2001; Ribberink et al., 2008). Oscillatory flow tunnels emulate wave boundary layer conditions. The vertical velocity component of waves diminishes towards the seabed. As a result, water motion at the bed is oscillatory (Jonsson and Carlsen, 1976). Near-bed hydrodynamics of storm waves can thus be generated by imposing the representative oscillatory velocity and orbital excursion length. The traditional U-tube flume design was adapted to be *i)* able to measure the erodibility of tidal flat sediments specifically, *ii)* transportable and useable outside of a laboratory, i.e., in the field or on a ship, *iii)* able to create a smooth flume channel – sediment transition with minimal disturbance to the sediment and *iv)* enable conducting a high number of erodibility measurements within a short time period. Besides these practical considerations, the flume also needs to be able to generate the high oscillatory velocities which are typically needed to erode cohesive sediments.

The OsCaR-flume (Fig. 1A) consists of two acrylic vertical tubes (2 m long, 0.09 m internal diameter) attached to a stainless steel channel (internal dimensions $l \times w \times h = 1.5 \times 0.21 \times 0.03$ m, Fig. 1C). The vertical tubes and channel are attached to a stainless-steel frame, to prevent flexing and vibrations. The cross-sectional flow area of the vertical tubes and the channel are equal in order to avoid flow velocity gradients. Gradients in wetted perimeter are minimized by a gradual transition from the round vertical tubes to the rectangular channel. A sediment core can be pushed into a 0.2×0.125 m opening in the bottom of the flume channel (Fig. 1D and E), which represents a similar disturbance to pushing a field device into the sediment from above. To ensure a watertight seal and to create a smooth interface between the flume channel and the sediment bed, the sediment core is placed inside a box with clay (Fig. 1D). As the outer shell of the sediment core is pushed against the bottom of the flume channel it is pushed into the clay, creating a watertight seal. This pushes the sediment up from the core and into the channel, creating a smooth transition between the flume channel and sediment (Fig. 1E), so that edge effects are minimized. Oscillatory flow is generated using a pneumatically operated piston, which is identical in hydrodynamic control to the TiDyWAVE field flume (de Smit et al., 2020) and therefore operable at field sites using either a compressor or dive bottle for compressed air. The piston is fully submerged in order to obtain a vacuum, which is achieved by sealing the tube – piston interface with rubber O-rings. This ensures that the water motion follows the movement of the pneumatic piston without added effects of gravitational return flow. The oscillatory velocity can be adjusted by adjusting the air input flowrate. A Programmable Logic Controller (PLC, Siemens LOGO) is used to control a proportional directional control valve (Festo MPYE series), i.e., a pneumatic valve of which both flow direction and velocity can be digitally controlled, thereby tightly controlling the oscillation of the pneumatic piston. Wave period and asymmetry can be adjusted by adjusting the open-closing cycle rate and maximum opening of the valve programmatically (Figure A1).

2.2. Determining sediment resuspension thresholds and critical bottom shear stress

Sediment erodibility is measured by gradually increasing the oscillatory flow in small increments until sediment resuspension is observed. Observation of sediment resuspension is done both visually, which is a typical method for quantifying sediment resuspension thresholds (see e.g. de Smit et al., 2020; van Rijn, 2020), and using a turbidity sensor in order to obtain an objective criterium (Fig. 2, Figure A2). The turbidity sensor (Turner Cyclops 7) is placed 0.3 m away from the sediment to

Fig. 1. The OsCaR-flume (A) is a U-tube type flume where a piston (B) forces oscillatory flow through a shallow channel (C). The flume and channel are secured by a metal frame to prevent vibrations from the movement of the piston. The sediment core is placed on top of a clay bed, which is used to make a watertight seal at the bottom of the sediment core (D). By pushing the sediment core into the clay bed the sediment can be raised out of the core and into the flume channel to ensure a smooth transition between the bottom of the flume channel and the sediment (E). Colored outlines in (A) correspond to outlines of closeups (B–E).

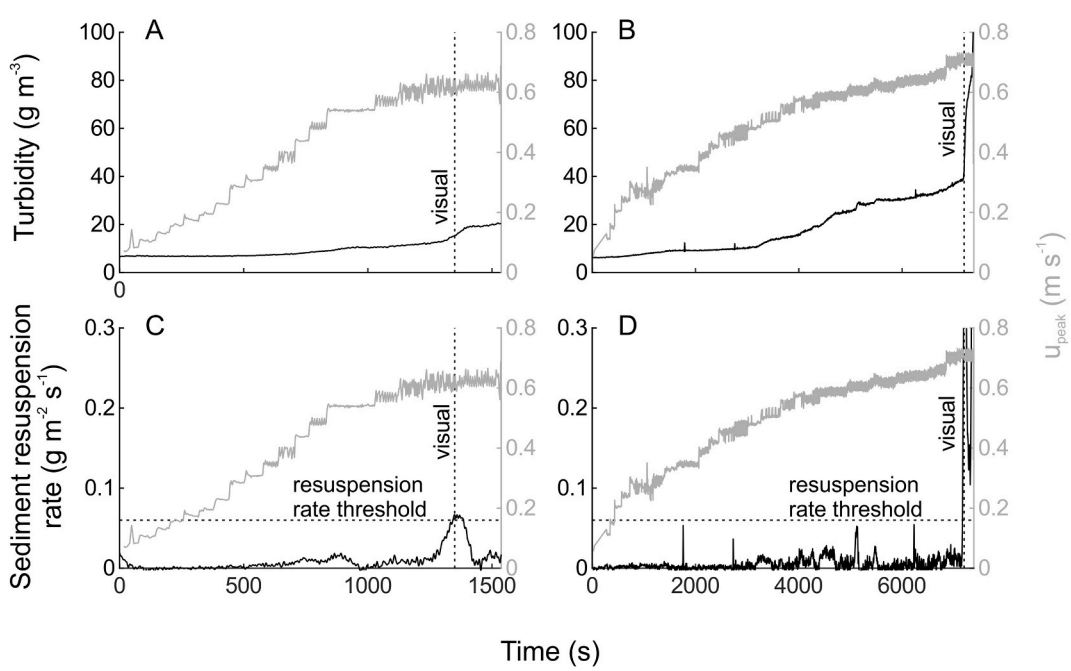

Fig. 2. *Example of determining the critical oscillatory velocity (u_{cr}) from both visual observations (moment indicated by vertical black line) and the sediment resuspension rate derived from the turbidity signal (threshold indicated by horizontal black line). A,C) shorter measurement with a relatively fast increase in u_{peak}. B,D) longer measurement with a slow increase in u_{peak} on the same sediment. While turbidity is much higher (A,B), exceedance of the threshold sediment resuspension rate occurs at a similar u_{peak} (C,D).*

avoid interference with the oscillatory flow above the sediment core (Fig. 1A,C). Erosion of muddy sediments can be divided into roughly two stages: *i)* erosion of loose bed material, flocs, and organic material present on the sediment surface, which is associated with type 1 erosion and *ii)* erosion of the cohesive sediment underneath, which is associated with type 1b or type 2 erosion (Amos et al., 1992). Here, the sediment resuspension threshold is defined as the latter. Given that the amount of sediment available for type 1 erosion can vary and that type 1 and type 2 erosion can occur simultaneously, turbidity cannot be used directly to quantify the sediment resuspension threshold (Fig. 2A and B). From comparison between visual observations and turbidity levels, the first derivative of the turbidity signal, i.e., the sediment resuspension rate, was found to be a consistent indicator for the onset of erosion of the cohesive sediment (Fig. 2C and D). That is, a script would detect a peak in the sediment resuspension rate, at the same time we visually observed the onset of erosion (Figure A2). The derived threshold varies somewhat depending on the properties of the mud fraction, but is generally in the order of 0.06 g m^{-2} s^{-1}. In general, automatic detection of the onset of erosion is possible when the mud fraction is sufficient, while visual observation has to be used for sandy sediments (Figure A2).

The oscillatory flow velocity cannot be measured directly due to the small internal dimensions of the channel. Therefore, a 25 Hz pressure sensor (Drück, 1800 series) is placed in the open-ended vertical tube to measure the vertical water motion (Fig. 1A). As water is virtually incompressible and flow area of the tubes and flume channel are equal, it can be assumed that the flow velocity is equal to the first derivative of the pressure signal (in mH_2O). The pressure signal was filtered using a 5th order Butterworth filter to remove frequencies below 0.05 Hz and frequencies above 0.5 Hz to filter out respectively changes in mean pressure and small pressure peaks and noise. As the OsCaR-flume can generate both symmetric and asymmetric oscillatory flow, u_{cr} was defined as the average of the peak oscillatory velocities of each wave cycle over a 1 min period.

The critical bottom shear stress generated by the OsCaR-flume (τ_{cr}) was calculated from the measured u_{cr} in order to obtain an equal comparison across sediment types and bed configurations (Le Hir et al., 2007). τ_{cr} was calculated as:

$$\tau_{cr} = \frac{1}{2}\rho f_w {u_{cr}}^2 \quad [2]$$

where ρ is the water density (1027 kg m^{-3} for seawater) and f_w is a dimensionless friction factor which for natural waves is calculated as (Soulsby, 1997):

$$f_w = 1.39\left(\frac{A_{max}}{\frac{1}{30}k_s}\right)^{-0.52} \quad [3]$$

where $A_{\max}$ is the wave orbital excursion length (m), which for the OsCaR-flume is the length of the oscillation of the pneumatic piston, and k_s is the bed roughness (m). However, given that the sediment core only makes up a small portion of the flume channel, *ks* is taken as a constant flume property, reducing eq. (3) to:

$$f_w = a{A_{max}}^{-0.52} \quad [4]$$

where a is a constant (−), which was determined from u_{cr} measurements on sand (D_{50} = 340 μm) with a known τ_{cr} of 0.2 N m^{-2} following from the Shields curve (Soulsby, 1997). Measured u_{cr} of this sediment was 0.15 m s^{-1} with a corresponding $A_{\max}$ of 0.22 m. This yields a f_w of 0.017 following eq. (2), and a constant a of 0.0076 following eq. (4). The f_w value is a typical value for rough turbulent flow (Jonsson, 1966), which is the expected turbulence regime in the OsCaR flume given that the flow Reynolds number exceeds 4000 at $u > 0.08$ m s^{-1} (Figure A3, Hino et al., 1976). The value of the constant a equates to a *ks* value in the order of 1 mm, which is a typical roughness height for a flat seabed. Given that $A_{\max}$ is proportional to both u_{cr} and to the wave period (T), which can both be adjusted independently in the OsCaR-flume, erodibility measurements on a coarse sand (τ_{cr} = 0.65 N m^{-2}) were conducted for a range of wave periods from $T = 3$ s to $T = 8$ s in order to assess whether eq. (4) is generally applicable for the OsCaR-flume across a range of typical wave periods.

2.3. Assessing hydrodynamic accuracy of the OsCaR-flume

Due to the small inner dimensions of the flume channel, it was not possible to take direct measurements of the flow structure inside the OsCaR flume. Therefore, to test whether the OsCaR-flume is able to generate near-bed hydrodynamics which accurately correspond to those of natural waves, sediment erodibility was measured for defaunated sand – mud mixtures of which the erodibility can be calculated from theory. Existing theory is derived from erodibility measurements conducted in hydrodynamically more advanced flumes, which have been proven to yield reliable results. Hence, a good correspondence between measured and calculated erodibility implies that the hydrodynamic simplifications posed by the OsCaR-flume design do not significantly impair its hydrodynamic performance, and thereby its ability to measure the erodibility of natural sediments. The sand – mud mixtures consisted of various combinations of pure sand (D_{50} = 340 μm, 0% mud content) and a muddy sediment (D_{50} = 32 μm, 66.5% mud content). Erodibility measurements were conducted on the pure sand and muddy sediment, and on 6 sand – mud mixtures with a mud content ranging between 4% and 57% (Table 1). The wave period in the OsCaR-flume was set at $T = 4$ s, which corresponds to typical waves in fetch-limited systems such as estuaries and shallow bays.

For the sand – mud mixtures, τ_{cr} as measured in the OsCaR-flume was compared with τ_{cr} calculated from the grain size distribution and mud content, using empirical predictors of van Ledden (2003) and Wu et al. (2018). van Ledden, 2003 assumes a near linear increase in τ_{cr} with increasing mud content with an inflection point at the critical mud content for the onset of cohesion, which is 5% clay volume which translates to a 20% critical mud content for the tested mixtures van Ledden (2003):

$$\begin{cases} \tau_{cr,ledden} = \tau_{cr,sand}(1+p_m)^{\beta} \quad if\ p_m < p_{mc} \\ \tau_{cr,ledden} = \dfrac{\tau_{cr,sand}(1+p_{mc})^{\beta} - \tau_{cr,mud}}{1-p_{mc}}(1-p_m) + \tau_{cr,mud}\ if\ p_m > p_{mc} \end{cases} \quad [5]$$

where p_m and p_s are the relative mud and sand concentrations respectively, p_{mc} is the critical mud content for the onset of cohesion, $\tau_{cr,sand}$ and $\tau_{cr,mud}$ are the critical bottom shear stress for pure sand and muddy sediment, and β is an empirical factor between 0.75 and 1.25.

Wu et al. (2018) assume a nonlinear relation between mud content and τ_{cr} of the sand – mud mixture:

$$\tau_{cr,wu} = \tau_{cr,lowpm} + (\tau_{cr,mud} - \tau_{cr,lowpm})\exp\left[-\alpha\left(\frac{p_s}{p_m}\right)^{1.2}\right] \quad [6]$$

where α is a factor based on the median grain size of the sand fraction,

Table 1
Sediment properties of the sand-mud mixtures used for the hydrodynamic assessment of the OsCaR-flume.

	D_{50} (μm)	D_{90} (μm)	% mud
Mud	32	142	66.5
Mix 1	47	336	57.0
Mix 2	148	490	39.0
Mix 3	291	546	20.9
Mix 4	297	551	19.9
Mix 5	330	536	11.7
Mix 6	344	524	3.9
Sand	341	493	0

and $\tau_{cr,lowpm}$ is the critical bottom shear stress for mud concentrations (p_m) below 5% mud volume. α is calculated as:

$$\alpha = 0.42\exp\left(-0.004D_{50,sand}\right) \quad [7]$$

where $D_{50,sand}$ is the median grain size of the sand fraction (m). $\tau_{cr,lowpm}$ is calculated as (Wu et al., 2018):

$$\tau_{cr,lowpm} = \tau_{cr,sand} + 1.25\left(\tau_{cr,mud} - \tau_{cr,sand}\right)\min(p_m, 0.05) \quad [8]$$

Both van Ledden (2003) and Wu et al. (2018) require $\tau_{cr,sand}$ (0.2 N m^{-2} in this study) and $\tau_{cr,mud}$ as input parameters. $\tau_{cr,mud}$ depends on the degree of consolidation of the sediment, i.e., its solid/void volume ratio, and therefore it can only be experimentally determined for a specific natural sand-mud mixture. Wu et al. (2018) derived a solid/void volume ratio – $\tau_{cr,mud}$ regression based on carefully selected erodibility measurements on muddy sediments from literature, $\tau_{cr,mud} = 10.29r^{1.7}$, where r is the solid/void volume ratio (−) of the mud fraction. Wu et al. (2018) propose the following equations to derive the solid/void volume ratio:

$$\frac{1}{\rho_d} = \frac{p_s}{\rho_s}B + \frac{p_s}{\rho_{ds}}(1-B) + \frac{p_m}{\rho_{dm}} \quad [9]$$

where ρ_d, ρ_{ds}, and ρ_{dm} are the dry bulk densities (kg m^{-3}) of the sediment mixture (1000 kg m^{-3} for the muddy sediment), the sand fraction (1600 kg m^{-3}), and mud fraction, respectively. B is a filling coefficient (−), which is 0.65 for a less compacted sand – mud mixture with sufficient mud content to fill the gaps between sand particles. This yields a mud fraction dry bulk density of 787 kg m^{-3}. The solid/void ratio of the mud fraction can be calculated from its dry bulk density as:

$$r = \frac{1-\varphi_m}{\varphi_m},\ \varphi_m = 1 - \frac{\rho_{dm}}{\rho_s} \quad [10]$$

where Φ_m is the muddy sediment porosity (−), yielding a solid/void volume ratio of 0.42 for the muddy sediment, resulting in a $\tau_{cr,mud}$ of 2.37 N m^{-2} for the defaunated sand – mud mixtures.

2.4. Real world testing: measuring erodibility along a natural mud – sand gradient

To verify whether the OsCaR-flume is indeed able to measure natural gradients in erodibility of tidal flat sediments, a small measurement campaign was conducted during two days in June 2019 in the Mokbaai tidal basin on the Texel island, located in the Dutch part of the Wadden Sea (Fig. 3). Sediment cores (l × w × h = 0.225 × 0.15 × 0.08 m) were collected during low tide on along a naturally occurring mud-sand gradient from the base towards the mouth of the tidal basin (Fig. 3). At each site, 5 sediment cores were taken. The cores were gently pushed into the sediment until approximately 5 mm of the core remained above the sediment surface, so that porewater would not flow out from the sides when digging out the sediment cores. The cores were then dug out carefully from the sides, after which a thin metal sheet was slid underneath, enabling the cores to be carefully lifted from the sediment and placed in the clay box. By following this procedure disturbance of the sediment surface is minimized by limiting movement and friction to the sides of the sediment core and deeper sediment layers only (Fig. 4). As the sediment cores extend 1.25 cm from the opening in the OsCaR-flume, the area mostly affected by digging out the sediment core can be excluded from the flume measurements. The cores were carefully transported to the OsCaR-flume, which was placed 2 km away from the furthest sampling location, following the method of Tolhurst et al. (2000). On the tidal flat, cores were transported by sleds, and transport by car was limited to 1 km in order to minimize disturbance due to vibrations. Upon arrival at the OsCaR-flume, the sediment cores were covered with a thin layer of seawater to avoid desiccation, and left for at least 1 h to reconsolidate. τ_{cr} was measured on the same day and compared with calculated τ_{cr} following the previously described method. The effect of these disturbances to the sediment erodibility is negligible (Tolhurst et al., 2000).

At each site along the naturally occurring mud-sand gradient from the base towards the mouth of the tidal basin, also 4 benthic samples and 3 grain size samples were collected. Grain size samples were taken of the top 0.03 m sediment layer and analyzed for grain size distribution and mud content. Benthic macrofauna samples of the top 0.35 m sediment layer were taken using a 0.019 m^2 surface area corer. The material was sieved over a 1 mm square mesh sieve. Taxa were determined up to species level, and individual biomass was measured in ash free dry mass (AFDM). Subsequently, species were aggregated into functional groups following the classification of Queirós et al. (2013). Distinction was made between 1) sediment reworkers, 2) surface modifiers, 3) up- and downward conveyers, 4) burrowers, and 5) biostabilizers. The metabolic rate of an individual of each taxon I_{ind} (mW) was calculated using the empirical model of Brey (2010), assuming a water temperature of 18 °C. Conversion factors for AFDW to mass in Joule were obtained from (Brey

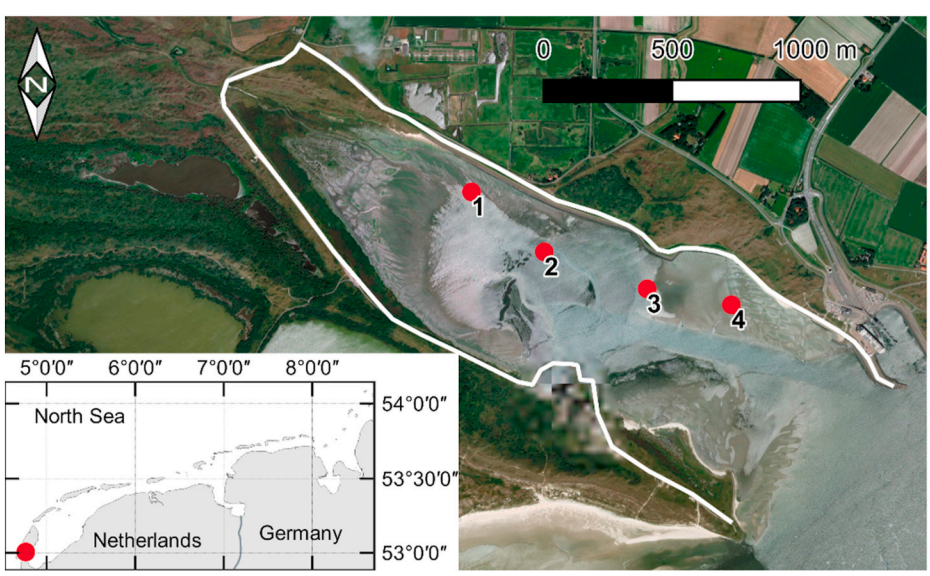

Fig. 3. Overview of the Mokbaai tidal basin (outlined in white) on the Texel island in the Dutch Wadden Sea. Sediment cores were taken along a natural mud-sand gradient from site 1 (muddy) to site 4 (sandy).

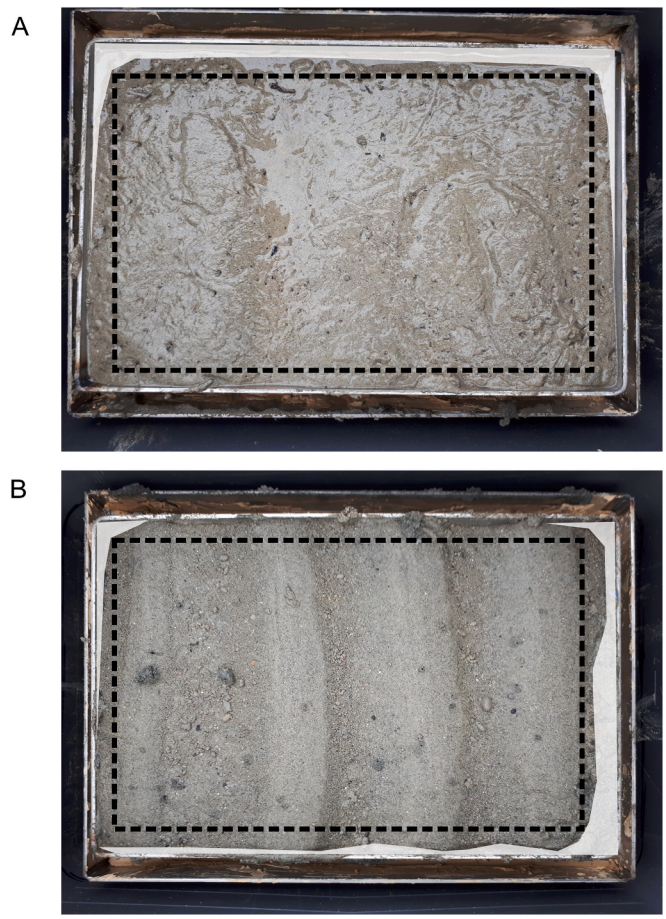

Fig. 4. Examples of sediment cores taken from the field. A) a muddy sediment with a high number of Corophium volutator individuals. B) a more sandy sediment containing wave ripples. Note that the loose, flocculated material behind the ripples is still present. The shaded areas indicate parts of the core which were visually disturbed due to collection and transport, and the dotted lines indicate the areas which are pushed into the OsCaR-flume.

et al., 2010). If there was no conversion factor available for a specific taxon, generic conversion factors were used based on motility and feeding behavior. The total benthic metabolic rate, I_{tot} (mW m^{-2}) was subsequently calculated for each functional group and was used as a proxy for the influence of benthic invertebrates on sediment erodibility (Cozzoli et al., 2018).

3. Results

3.1. Hydrodynamic assessment

Measurements on coarse sand (τ_{cr} = 0.65 N m^{-2}) using a range of orbital magnitudes by varying the wave period from T = 3 s to T = 8.5 s show that the friction factor f_w in the OsCaR-flume is correctly proportional to the orbital magnitude across a wide range of typical wave periods in coastal systems (Fig. 5). As the wave period increases so does the orbital excursion length, yielding a reduction in f_w and an increase in u_{cr} when τ_{cr} remains constant. Hence, eq. (4) may be used to determine f_w and the resulting bed shear stress in the OsCaR-flume.

We observed a good correlation between τ_{cr} measured in the OsCaR-flume and τ_{cr} calculated from theory in sediment mixtures without benthos (Fig. 6). The best fit was observed with the predictor of Wu et al. (2018), van Ledden (2003) underpredicts the increase in τ_{cr} of the sand fraction with mud contents below the onset of cohesion. This confirms that the OsCaR-flume is able to generate realistic shear stresses for a

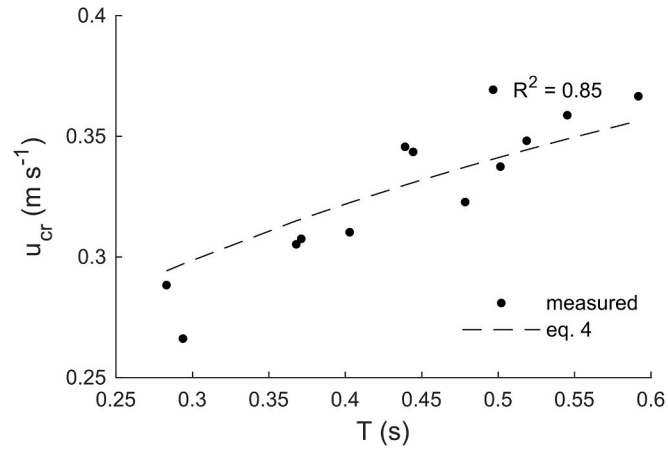

Fig. 5. Orbital magnitude against ucr for a coarse sand with τcr = 0.65 N m-2.

range of sediment types under both low energy (i.e., 0.2 N m^{-2} for pure sand, corresponding to a 0.16 m s^{-1} peak oscillatory velocity, which is typical for waves on tidal flats under calm conditions) and high energy conditions (i.e., 2.17 ± 0.31 N m^{-2} for 66.5% mud content, corresponding to a 0.66 ± 0.06 m s^{-1} peak oscillatory velocity, which is typical for waves on tidal flats under stormy conditions. Although $\tau_{cr,sand}$ is used as a fitting factor, the close correlation for intermediate mud contents and the good correspondence between measured and calculated τ_{cr} of the muddy sediment show that the increase of bottom shear stress generated by the OsCaR-flume is correctly proportional to the imposed increase in peak oscillatory velocity.

3.2. Erodibility along a natural mud-sand gradient

Sediments along the mud-sand gradient of the Mokbaai tidal basin varied considerably in grain size distribution, mud content, total metabolic rate of benthic macrofauna (Table 2), and benthic species (Table S1). Site 1 and 2 can be characterized as muddy, with mud volumes ranging from 24 to 58% and a finer sand fraction composition (D_{50} = 186 μm). Site 4 is predominantly sandy, with mud volumes of 7.24 ± 3.66% and a coarser sand fraction (D_{50} = 252 μm). Site 3 is transitional, with mud volumes similar to site 2 (22–23%) and sand composition similar to site 4 (D_{50} = 279 μm). Total benthic metabolic rates also varied considerably, with mean metabolic rates ranging from 0.81 mW m^{-2} for site 2 (i.e., extremely low benthic activity), 27.99–45.48 mW m^{-2} for site 1 and 4, and 179.85 mW m^{-2} for site 3 (Table 2, Fig. 7C).

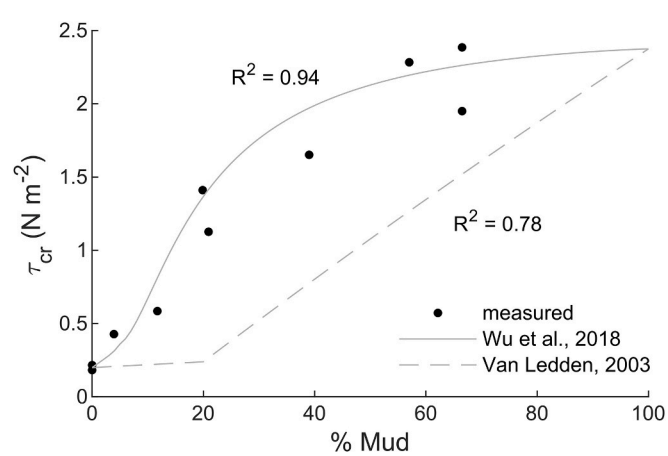

Fig. 6. τ_{cr} against mud percentage for defaunated sand-mud mixtures as measured in the OsCaR-flume compared with the empirical relation derived by van Ledden (2003) and Wu et al. (2018).

Table 2
Sediment characteristics and total metabolic rate for each measurement site. Values are reported as means ± SE. Complete taxonomic results are available in Table S1.

	D_{50} (μm)	D_{90} (μm)	% mud	$D_{50,sand}$ (μm)	I_{tot} (mW m^{-2})
Site 1	64 ± 9	254 ± 6	53.75 ± 4.62	187 ± 1	43.63 ± 9.52
Site 2	144 ± 9	323 ± 9	24.67 ± 0.75	191 ± 10	0.81 ± 0.68
Site 3	253 ± 6	374 ± 5	23.15 ± 3.29	280 ± 2	179.85 ± 70.08
Site 4	246 ± 4	357 ± 2	7.24 ± 3.66	252 ± 1	27.99 ± 15.69

Measurements with the OsCaR-flume revealed large differences in natural sediment erodibility of the Mokbaai tidal basin (Fig. 7A), which ranged between 0.11 ± 0.02 and 1.74 ± 0.14 N m^{-2} for respectively site 4 and site 2. Given the presence of benthos in the sediment affecting the bulk properties, eqs. (9) and (10) cannot be applied to calculate $\tau_{cr,mud}$. Instead, $\tau_{cr,mud}$ was estimated by fitting the predictor of Wu et al. (2018, eqs. (6)–(8)) to measured τ_{cr} at site 2, where total benthic metabolic rate was near 0. (Table 2). In this case $\tau_{cr,mud}$ was 3.5 N m^{-2}. At sites 1, 3, and 4, where total benthic metabolic rate was higher (Table 2, Fig. 7C), mean measured τ_{cr}, was 2.3–3.5 times lower than calculated τ_{cr} (Fig. 7A and B) as essentially calculated τ_{cr} is only valid for $I_{tot} = 0$. Relatively, this reduction in τ_{cr} did not vary significantly between the different sediment types and benthic assemblages (one-way ANOVA p = 0.27). The largest relative reduction in τ_{cr} was observed at site 4, which was predominantly sandy. The mud volume (7.24 ± 3.66%) was only slightly above the threshold where τ_{cr} starts to increase exponentially. Interestingly, the measured τ_{cr} (0.11 ± 0.02 N m^{-2}) approximates the calculated τ_{cr} of the sand fraction, which for this sediment is 0.17 N m^{-2} following from Shields theory. This indicates that the macrobenthos present were able to completely eradicate the effect of cohesion on the erodibility of this sediment, but were not able to alter the erodibility of the sand fraction. At site 1 and 3, mean measured τ_{cr} was respectively 2.2 and 2.7 times lower than calculated τ_{cr} (Fig. 7A). Relatively, this reduction in τ_{cr} did not vary significantly (Tukey-Kramer post-hoc p = 0.26). However, the total benthic metabolic rate was significantly higher at site 3 (Welch's T-test p = 0.008). This may indicate a potential threshold-type response of sediment erodibility to total benthic metabolic rate (Fig. 7B), albeit that this remains inconclusive given the variation in sediment composition between sites. Site 3 also showed a large variation in measured erodibility between the replicates (Fig. 7A). Differences between the replicated measurements of total benthic metabolic rate were also large, indicating that small-scale spatial heterogeneity of macrobenthic activity can cause similar patterns in sediment erodibility.

4. Discussion

In this study we show that the OsCaR-flume is able to generate bottom shear stress similar to that generated by natural waves. Consequently, the measured sediment erodibility was comparable with erodibility calculated from theory, both for a range of defaunated sand-mud mixtures and for a natural sediment with low benthic metabolic rate. Measurements along a natural longshore estuarine gradient showed considerable differences in sediment erodibility. These could be partly explained by the gradient in mud content, but the largest differences were related to differences in the density and species composition of benthic invertebrates, which the presented physical theory does not account for. Overall these results highlight the site specificity of tidal flat erodibility, and hence the need for methods like the OsCaR-flume to be able to rapidly quantify these differences, in order to understand tidal flat biogeomorphology.

4.1. Patterns in influence of benthos on sediment erodibility

Results from the field measurements show that the OsCaR-flume is able to measure key differences in erodibility of both benthic and sedimentary gradients, in that the observed patterns agree with previous

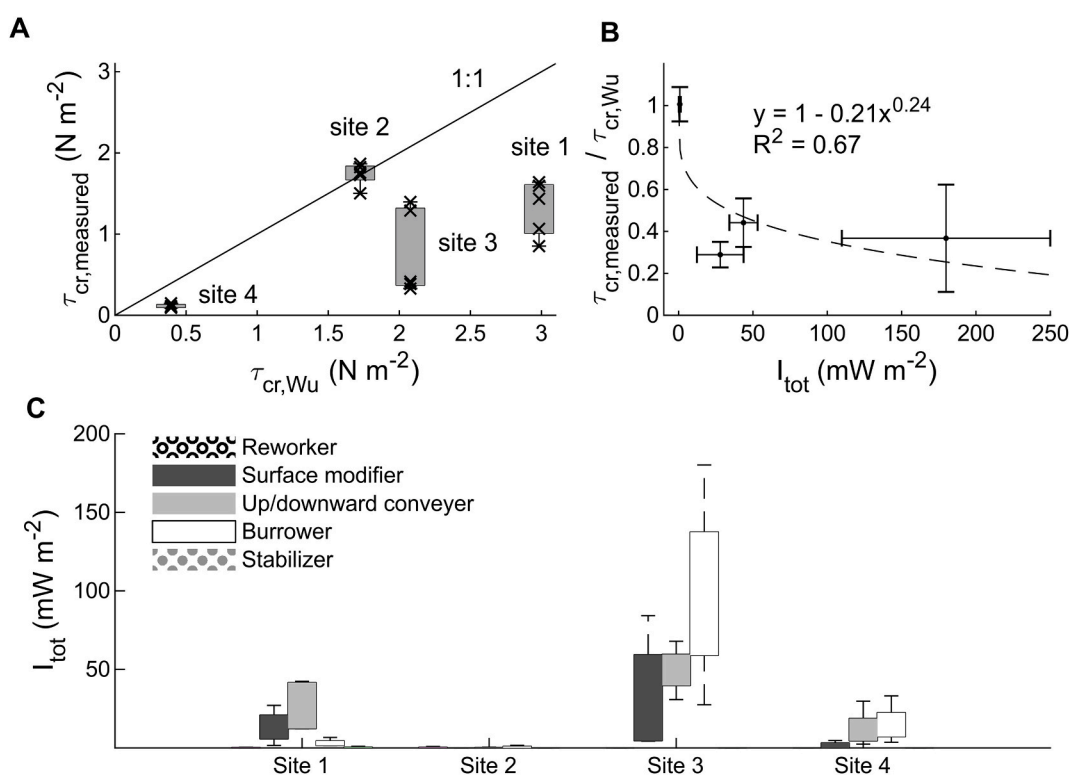

Fig. 7. A: Measured τ_{cr} plotted against $\tau_{cr,Wu}$, calculated based on sediment properties only according to Wu et al. (2018), with $\tau_{cr,mud}$ fitted to site 2, where total benthic metabolic rate was negligible. B: Effect of I_{tot} on the reduction of τ_{cr}, expressed as $\tau_{cr,measured}/\tau_{cr,Wu}$. This was nondimensionalized to correct for the different sediment types. C: Total metabolic rate I_{tot} of benthic species divided by type of behavior in relation to the sediment.

laboratory and field based studies. Li et al. (2017) observed that the presence and density of *Cerastoderma edule* did not change the erodibility or erosion rate of non-cohesive sediment, though a large effect of *Cerastoderma edule* on suspended sediment concentrations was found in sediments with low silt concentrations (Cozzoli et al., 2020). We did not observe a significant reduction in τ_{cr} beyond τ_{cr} of the sand fraction in a moderately cohesive sediment with a <10% mud content. This indicates that macrobenthic species can fully eradicate cohesiveness of these sediments, causing high concentrations of suspended muds in the water column, but do not significantly change the erodibility of the non-cohesive sand fraction. We also observed a threshold-type response of the reduction in sediment erodibility to total benthic metabolic rate, as there was little additional decrease in sediment erodibility beyond total benthic metabolic rates of approx. 30 mW m^{-2}. This is in agreement with for example the results of de Deckere et al. (2000), who observed a threshold in the decrease of critical flow velocities for sediment resuspension with increasing densities of *Corophium volutator*, and Cozzoli et al. (2019), who observed a threshold in the increase of equilibrium suspended sediment concentrations at a given bottom shear stress with increasing total benthic metabolic rate. The latter can be interpreted as a similar decrease in sediment erodibility.

4.2. Advantages and limitations of the OsCaR-flume

The OsCaR-flume is specifically designed to rapidly assess τ_{cr} of natural sediments. The field measurements presented in this paper, excluding sediment and benthos analyses, took approximately 12 h in total. As of yet, smaller devices such as shear vanes or small vertical tubes where turbulence is generated by rotating disks or vertical jets were used for rapid in situ τ_{cr} assessment of natural sediments. These methods only provide a proxy for the shear stress, and do not generate values that fit 1:1 with τ_{cr} when bottom shear stress is generated by natural flow or waves. For example, bed roughness has a major influence on τ_{cr} when flow is horizontal, i.e. for near-bed oscillatory currents under waves. However, bed roughness did not influence measured τ_{cr} using devices generating vertical shear stress. The latter generally resulted in unrealistically high τ_{cr} values (Widdows et al., 2007). Using vertical shear stress to measure τ_{cr} may also cause underrepresentation of the effect of benthos, as the alteration of bed roughness is an important mechanism through which benthic macrofauna influence τ_{cr} (Le Hir et al., 2007). This makes these devices less suitable for the detailed quantification of τ_{cr} that is needed for predicting the morphological development of tidal flats (Orvain et al., 2012). By generating a horizontal shear stress, the OsCaR-flume is more realistic in terms of mimicking natural wave dynamics.

In the OsCaR-flume the orbital magnitude of the imposed waves increases with increasing peak orbital velocities, and is larger than the length of the sediment core. Therefore, the turbidity signal cannot directly be translated to the amount of sediment that is resuspended from the sediment core, as it is also influenced by mixing and diffusion. In addition, despite the possibility of pushing the sediment core further upwards, the transition between the flume channel and sediment core will likely induce edge effects when a significant amount of sediment is eroded. As a result, the erosion parameter that describes the erosion rate once τ_{cr} is exceeded (E_0, kg m^{-2} s^{-1}; see eq. (1)) cannot be determined sufficiently accurate. This would require e.g. an annular flume, for which the length of the seabed is essentially infinite. Similar to τ_{cr}, E_0 has a large spatiotemporal variation on tidal flats (Amos et al., 2010), and therefore it is an important parameter to measure as well. Although this is a clear limitation of the OsCaR-flume, the effect of τ_{cr} on the erosion of cohesive sediments changes not only the shear stress at which erosion occurs, and thus the duration of an erosion event, but also the erosion rate at a given shear stress. Significant changes in τ_{cr}, especially toward lower values, lead to an exponentially increasing amount of erosion over a tidal cycle (Figure A4). However, the effect of errors in the erosion parameter E_0 becomes increasingly larger when considering extreme erosion events where deeper sediment layers become exposed, and when variations in both τ_{cr} and E_0 are small their effect on total erosion is similar. Hence, measurements of both τ_{cr} and E_0 using specialized devices for each would be most ideal.

5. Outlook

While being mobile and operable at field sites, in order to limit the transport of sediment samples to an extent where it does not influence erodibility (cf. Tolhurst et al., 2000), the OsCaR-flume is not technically a field flume. It is not placed in the field on undisturbed sediment, though placing a field flume of the size needed to obtain sufficiently accurate hydrodynamics is a sediment disturbance in itself. The OsCaR-flume aims to fill the gap between laboratory-based facilities, which limit potential study sites based on where they are located, and field flumes, which due to their specific logistical challenges are better suited for in situ process measurements. In addition, it alleviates some practical challenges. Fieldwork is only limited to collecting sediment and benthos cores. This is especially advantageous when conducting erodibility measurements on the low-lying areas of tidal flats with short emergence times, i.e., the most dynamic areas where these measurements are most beneficial, as collecting samples for a full day of flume measurements can be done in well under 2 h. The OsCaR-flume may therefore be used to rapidly quantify τ_{cr} in relation to e.g., (inter)annual patterns in tidal flat stability at the estuary scale (cf. Widdows et al., 2000), sediment stability thresholds for saltmarsh establishment or loss (cf. Hu et al., 2015; Bouma et al., 2016), or the stability of dredged sediments (cf. Widdows et al., 2006). These kind of measurements are crucial for the validation of morphodynamical models, which are becoming more detailed, but also more complex, by including dynamic flow – vegetation interactions and biota effects on sediment stability (Brückner et al. 2019, 2020, 2020; Cozzoli et al., 2021). In addition, similar to annular flumes, the OsCaR-flume can also be used for laboratory-based studies. For example, experimental assessment of the effect of specific species and individual densities on sediment resuspension (cf. Cozzoli et al., 2018, 2019). Such experiments will be done much faster using the OsCaR flume, allowing for experimental designs requiring a higher number of measurements, such as e.g. inclusion of various benthic communities (de Smit et al., 2021) or sediment mud contents representative of the studied system.

Declaration of competing interest

The authors declare that they have no known competing financial interests or personal relationships that could have appeared to influence the work reported in this paper.

Acknowledgements

The OsCaR-flume was originally designed by Tjeerd Bouma and Bert Sinke, built by the technical workshop of the NIOZ, and tested and optimized in hydrodynamics and pneumatic control by Jaco de Smit. We thank Rob Dekker, Loran Kleine Schaars, and the students of the NCK summer school 2019 for assistance with the Mokbaai fieldwork taxonomic identification of benthos, and sediment analyses. We thank Peter van Breugel for conducting the sediment analysis of the defaunated sand-mud mixtures. All data supporting this research and scripts for determining erosion thresholds and conducted the presented analyses are available at DOI: 10.4121/14572056. For more information on building the OsCaR-flume, please contact tjeerd.bouma@nioz.nl.

Appendix

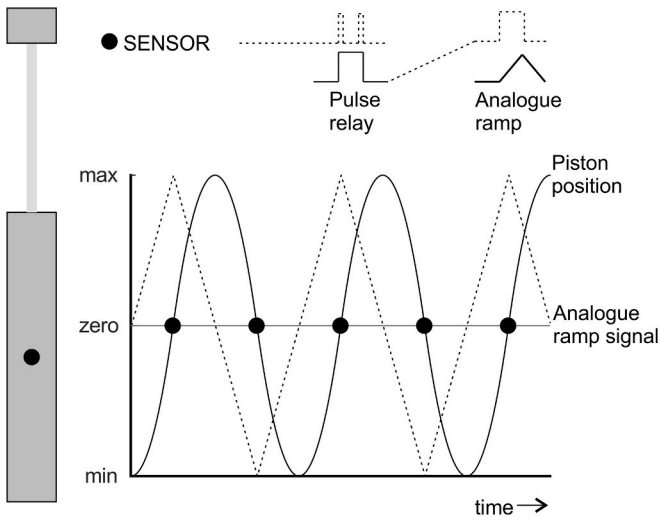

Figure A1. Operation scheme of the pneumatic piston. When starting up the flume, an analogue ramp signal is started in the PLC program, opening the pneumatic valve gradually and causing the piston to move outwards with increasing speed. A sensor emits a pulse signal once the piston has reached the middle (zero) position, prompting the analogue signal to revert. This slows down and ultimately reverts the piston with increasing speed. Thereby the sawtooth-shaped opening and closing cycle of the pneumatic valve results in a sinusoidal motion of the piston.

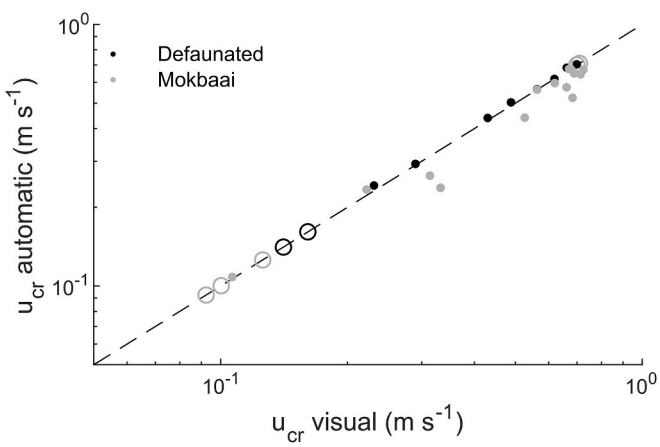

Figure A2. *Comparison between u_{cr} derived from visual observations and automatically determined u_{cr} using sediment resuspension rate derived from the turbidity signal as a proxy for the onset of sediment transport. Note that for sandy sediments, u_{cr} can only be determined visually due to a lack of suspendable sediments (open points).*

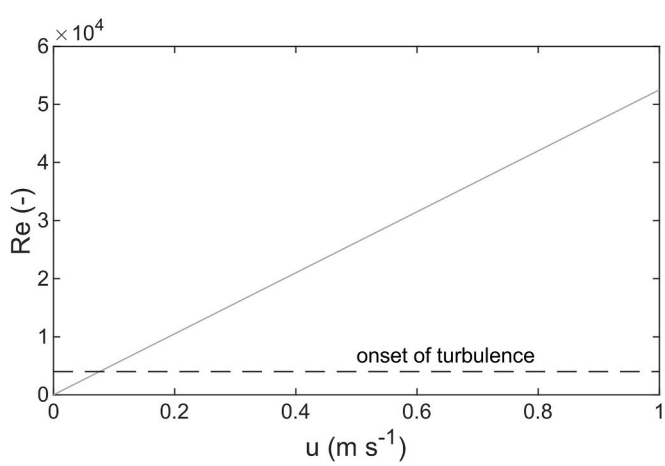

Figure A3. Flow Reynolds number against velocity. The flow is turbulent (conservatively estimated at Re > 4000) for velocities above 0.08 m s^{-1}, which is the minimum peak orbital velocity that can be generated in the OsCaR-flume.

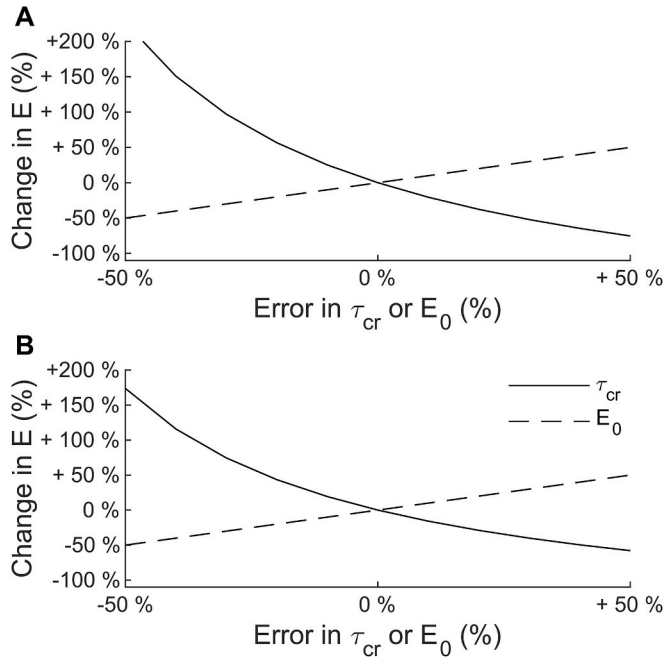

Figure A4. Effect of changes in τ_{cr} and E_0 on the total amount of erosion calculated using eq. (1) over a single tidal cycle under calm (A) and stormy (B) conditions for a conceptual tidal flat with 60% immersion time, a 2 m tidal amplitude, 0.35 m s^{-1} peak tidal flow, and a 0.15 m wave height under calm conditions and a 0.4 m wave height under stormy conditions. Calculations are available online, DOI: 10.4121/14572056.

References

Amos, C.L., Grant, J., Daborn, G.R., Black, K., 1992. Sea Carousel-A benthic, annular flume. Estuar. Coast Shelf Sci. 34, 557–577. https://doi.org/10.1016/S0272-7714(05)80062-9.

Amos, C.L., Umgiesser, G., Ferrarin, C., Thompson, C.E.L., Whitehouse, R.J.S., Sutherland, T.F., Bergamasco, A., 2010. The erosion rates of cohesive sediments in Venice lagoon. Italy. Cont. Shelf Res. 30, 859–870. https://doi.org/10.1016/j.csr.2009.12.001.

Bouma, T.J., van Belzen, J., Balke, T., others, 2016. Short-term mudflat dynamics drive long-term cyclic salt marsh dynamics. Limnol. Oceanogr. 61, 2261–2275. https://doi.org/10.1002/lno.10374.

Braat, L., Van Kessel, T., Leuven, J.R.F.W., Kleinhans, M.G., 2017. Effects of mud supply on large-scale estuary morphology and development over centuries to millennia. Earth Surf. Dyn. 5, 617–652. https://doi.org/10.5194/esurf-5-617-2017.

Brey, T., 2010. An empirical model for estimating aquatic invertebrate respiration. Methods Ecol. Evol. 1, 92–101. https://doi.org/10.1111/j.2041-210x.2009.00008.x.

Brey, T., Müller-Wiegmann, C., Zittier, Z.M.C., Hagen, W., 2010. Body composition in aquatic organisms - a global data bank of relationships between mass, elemental composition and energy content. J. Sea Res. 64, 334–340. https://doi.org/10.1016/j.seares.2010.05.002.

Brückner, M.Z.M., Braat, L., Schwarz, C., Kleinhans, M.G., 2020. What came first, mud or biostabilizers? Elucidating interacting effects in a coupled model of mud, saltmarsh, microphytobenthos, and estuarine morphology. Water Resour. Res. 56 https://doi.org/10.1029/2019wr026945.

Brückner, M.Z.M., Schwarz, C., Coco, G., Baar, A., Boechat Albernaz, M., Kleinhans, M.G., 2021. Benthic species as mud patrol - modelled effects of bioturbators and biofilms on large-scale estuarine mud and morphology. Earth Surf. Process. Landforms 1–17. https://doi.org/10.1002/esp.5080.

Brückner, M.Z.M., Schwarz, C., van Dijk, W.M., van Oorschot, M., Douma, H., Kleinhans, M.G., 2019. Salt marsh establishment and eco-engineering effects in dynamic estuaries determined by species growth and mortality. J. Geophys. Res. Earth Surf. 124, 2962–2986. https://doi.org/10.1029/2019JF005092.

Cozzoli, F., Bouma, T.J., Ottolander, P., Lluch, M.S., Ysebaert, T., Herman, P.M.J., 2018. The combined influence of body size and density on cohesive sediment resuspension by bioturbators. Sci. Rep. 8, 1–12. https://doi.org/10.1038/s41598-018-22190-3.

Cozzoli, F., Bouma, T.J., Ysebaert, T., Herman, P.M.J., 2013. Application of non-linear quantile regression to macrozoobenthic species distribution modelling: comparing two contrasting basins. Mar. Ecol. Prog. Ser. 475, 119–133. https://doi.org/10.3354/meps10112.

Cozzoli, F., Gjoni, V., Del Pasqua, M., others, 2019. A process based model of cohesive sediment resuspension under bioturbators' influence. Sci. Total Environ. 670, 18–30. https://doi.org/10.1016/j.scitotenv.2019.03.085.

Cozzoli, F., Gomes da Conceição, T., Van Dalen, J., others, 2020. Biological and physical drivers of bio-mediated sediment resuspension: a flume study on Cerastoderma edule. Estuar. Coast Shelf Sci. 241 https://doi.org/10.1016/j.ecss.2020.106824.

Cozzoli, F., Shokri, M., Gomes, T., others, 2021. Science of the Total Environment Modelling spatial and temporal patterns in bioturbator effects on sediment resuspension : a biophysical metabolic approach. Sci. Total Environ. 792, 148215. https://doi.org/10.1016/j.scitotenv.2021.148215.

de Deckere, E.M.G.T., van de Koppel, J., Heip, C.H.R., 2000. The influence of Corophium volutator abundance on resuspension. Hydrobiologia 426, 37–42. https://doi.org/10.1023/A:1003978714382.

Hino, M., Sawamoto, M., Takasu, S., 1976. Experiments on transition to turbulence in an oscillatory pipe flow. J. Fluid Mech. 75, 193–207. https://doi.org/10.1017/S0022112076000177.

Le Hir, P., Monbet, Y., Orvain, F., 2007. Sediment erodability in sediment transport modelling: can we account for biota effects? Continent. Shelf Res. 27, 1116–1142. https://doi.org/10.1016/j.csr.2005.11.016.

Houwing, E.J., Van Rijn, L.C., 1998. In Situ Erosion Flume (ISEF): determination of bed-shear stress and erosion of a kaolinitc bed. J. Sea Res. 39, 243–253. https://doi.org/10.1016/S1385-1101(98)00007-0.

Hu, Z., Van Belzen, J., Van Der Wal, D., Balke, T., Wang, Z.B., Stive, M., Bouma, T.J., 2015. Windows of opportunity for salt marsh vegetation establishment on bare tidal flats: the importance of temporal and spatial variability in hydrodynamic forcing. J. Geophys. Res. G Biogeosciences 120, 1450–1469. https://doi.org/10.1002/2014JG002870.

Joensuu, M., Pilditch, C.A., Harris, R., Hietanen, S., Pettersson, H., Norkko, A., 2018. Sediment properties, biota, and local habitat structure explain variation in the erodibility of coastal sediments. Limnol. Oceanogr. 63, 173–186. https://doi.org/10.1002/lno.10622.

Jonsson, I.G., 1966. Wave boundary layers and friction factors. Coast. Eng. Proc. 1, 9. https://doi.org/10.9753/icce.v10.9.

Jonsson, I.G., Carlsen, N.A., 1976. Experimental and theoretical investigations in an oscillatory turbulent boundary layer. J. Hydraul. Res. 14, 45–60. https://doi.org/10.1080/00221687609499687.

van Ledden, M., 2003. Sand-mud segregation in estuaries and tidal basins. Delft University of Technology, Delft.

Li, B., Cozzoli, F., Soissons, L.M., Bouma, T.J., Chen, L., 2017. Effects of bioturbation on the erodibility of cohesive versus non-cohesive sediments along a current-velocity gradient: a case study on cockles. J. Exp. Mar. Biol. Ecol. 496, 84–90. https://doi.org/10.1016/j.jembe.2017.08.002.

Mariotti, G., Fagherazzi, S., 2010. A numerical model for the coupled long-term evolution of salt marshes and tidal flats. J. Geophys. Res. Earth Surf. 115, 1–15. https://doi.org/10.1029/2009JF001326.

Mehta, A.J., Hayter, E.J., Parker, W.R., Krone, R.B., Teeter, A.M., 1989. Cohesive sediment transport. I: process description. J. Hydraul. Eng. 115, 1076–1093. https://doi.org/10.1061/(ASCE)0733-9429 (1989)115:8(1076).

Mitchener, H., Torfs, H., 1996. Erosion of mud/sand mixtures. Coast. Eng. 29, 1–25. https://doi.org/10.1016/S0378-3839(96)00002-6.

O'Donoghue, T., Clubb, G.S., 2001. Sand ripples generated by regular oscillatory flow. Coast. Eng. 44, 101–115. https://doi.org/10.1016/S0378-3839(01)00025-4.

Orvain, F., Le Hir, P., Sauriau, P.G., Lefebvre, S., 2012. Modelling the effects of macrofauna on sediment transport and bed elevation: application over a cross-shore mudflat profile and model validation. Estuar. Coast Shelf Sci. 108, 64–75. https://doi.org/10.1016/j.ecss.2011.12.036.

Partheniades, 1965. Erosion and deposition of cohesive soils. J. Hydraul. Div. 91, 105–139.

Paterson, D.M., Black, K.S., 1999. Water flow, sediment dynamics and benthic biology. In: Advances in Ecological Research, pp. 155–193.

Queirós, A.M., Birchenough, S.N.R., Bremner, J., others, 2013. A bioturbation classification of European marine infaunal invertebrates. Ecol. Evol. 3, 3958–3985. https://doi.org/10.1002/ece3.769.

Ribberink, J.S., van der Werf, J.J., O'Donoghue, T., Hassan, W.N.M., 2008. Sand motion induced by oscillatory flows: sheet flow and vortex ripples. J. Turbul. 9, N20. https://doi.org/10.1080/14685240802220009.

van Rijn, L.C., 2020. Erodibility of mud–sand bed mixtures. J. Hydraul. Eng. 146, 04019050 https://doi.org/10.1061/(asce)hy.1943-7900.0001677.

Schünemann, M., Kühl, H., 1993. Experimental Investigations of the Erosional Behavior of Naturally Formed Mud from the Elbe Estuary and Adjacent Wadden Sea, pp. 314–330. Germany.

de Smit, J.C., Brückner, M.Z.M., Mesdag, K.I., Kleinhans, M.G., Bouma, T.J., 2021. Key bioturbator species within benthic communities determine sediment resuspension thresholds. Front. Mar. Sci. 8, 726238 https://doi.org/10.3389/fmars.2021.726238.

de Smit, J.C., Kleinhans, M.G., Gerkema, T., Timmermans, K.R., Bouma, T.J., 2020. Introducing the TiDyWAVE field flume: a method to quantify natural ecosystem resilience against future storm waves. Limnol Oceanogr. Methods. https://doi.org/10.1002/lom3.10386.

Soulsby, R., 1997. Dynamics of Marine Sands: A Manual for Practical Applications. Thomas Telford Ltd.

Tolhurst, T.J., Black, K.S., Shayler, S.A., Mather, S., Black, I., Baker, K., Paterson, D.M., 1999. Measuring the in situ erosion shear stress of intertidal sediments with the cohesive strength meter (CSM). Estuar. Coast Shelf Sci. 49, 281–294. https://doi.org/10.1006/ecss.1999.0512.

Tolhurst, T.J., Riethmüller, R., Paterson, D.M., 2000. In situ versus laboratory analysis of sediment stability from intertidal mudflats. Continent. Shelf Res. 20, 1317–1334. https://doi.org/10.1016/S0278-4343(00)00025-X.

de Vet, P.L.M., van Prooijen, B.C., Colosimo, I., Steiner, N., Ysebaert, T., Herman, P.M.J., Wang, Z.B., 2020. Variations in storm-induced bed level dynamics across intertidal flats. Sci. Rep. 10, 1–15. https://doi.org/10.1038/s41598-020-69444-7.

Widdows, J., Brinsley, M.D., Pope, N.D., Staff, F.J., Bolam, S.G., Somerfield, P.J., 2006. Changes in biota and sediment erodability following the placement of fine dredged material on upper intertidal shores of estuaries. Mar. Ecol. Prog. Ser. 319, 27–41. https://doi.org/10.3354/meps319027.

Widdows, J., Brinsley, M.D., Salkeld, P.N., Elliott, M., 1998. Use of annular flumes to determine the influence of current velocity and bivalves on material flux at the sediment-water interface. Estuaries 21, 552. https://doi.org/10.2307/1353294.

Widdows, J., Brinsley, M., Salkeld, P., Lucas, C., 2000. Influence of biota on spatial and temporal variation in sediment erodability and material flux on a tidal flat (Westerschelde, The Netherlands). Mar. Ecol. Prog. Ser. 194, 23–37. https://doi.org/10.3354/meps194023.

Widdows, J., Friend, P.L., Bale, A.J., Brinsley, M.D., Pope, N.D., Thompson, C.E.L., 2007. Inter-comparison between five devices for determining erodability of intertidal sediments. Continent. Shelf Res. 27, 1174–1189. https://doi.org/10.1016/j.csr.2005.10.006.

Wu, W., Perera, C., Smith, J., Sanchez, A., 2018. Critical shear stress for erosion of sand and mud mixtures. J. Hydraul. Res. 56, 96–110. https://doi.org/10.1080/00221686.2017.1300195.

Yang, S.L., Friedrichs, C.T., Shi, Z., Ding, P.X., Zhu, J., Zhao, Q.Y., 2003. Morphological response of tidal marshes, flats and channels of the outer yangtze river mouth to a major storm. Estuaries 26, 1416–1425. https://doi.org/10.1007/BF02803650.

Ysebaert, T., Herman, P.M.J., 2002. Spatial and temporal variation in benthic macrofauna and relationships with environmental variables in an estuarine, intertidal soft-sediment environment. Mar. Ecol. Prog. Ser. 244, 105–124. https://doi.org/10.3354/meps244105.

Zhu, Q., van Prooijen, B.C., Maan, D.C., Wang, Z.B., Yao, P., Daggers, T., Yang, S.L., 2019. The heterogeneity of mudflat erodibility. Geomorphology 345, 106834. https://doi.org/10.1016/j.geomorph.2019.106834.